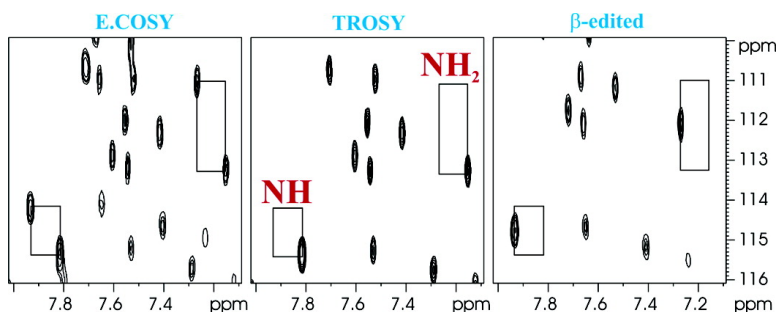


## Simultaneous Recording of Spin-State-Selective NMR Spectra for Different IS Spin Systems

Teodor Parella, and Margarida Gair

*J. Am. Chem. Soc.*, **2004**, 126 (31), 9821-9826 • DOI: 10.1021/ja0495866 • Publication Date (Web): 17 July 2004

Downloaded from <http://pubs.acs.org> on April 1, 2009



### More About This Article

Additional resources and features associated with this article are available within the HTML version:

- Supporting Information
- Access to high resolution figures
- Links to articles and content related to this article
- Copyright permission to reproduce figures and/or text from this article

[View the Full Text HTML](#)

## Simultaneous Recording of Spin-State-Selective NMR Spectra for Different $I_nS$ Spin Systems

Teodor Parella\*<sup>†</sup> and Margarida Gairi<sup>‡</sup>

Contribution from the Servei de Resonància Magnètica Nuclear, Universitat Autònoma de Barcelona, E-08193, Bellaterra, Spain, and Unitat de RMN d'Alt Camp, Serveis de Suport a la Recerca, Parc Científic de Barcelona, Universitat de Barcelona, C/ Josep Samitier, 1-5, E-08028, Barcelona, Spain

Received January 23, 2004; E-mail: teodor.parella@uab.es

**Abstract:** Heteronuclear magnetization transfer occurring during heteronuclear cross-polarization mixing processes in liquid-state NMR experiments can be easily monitored as a function of the involved in-phase, antiphase, and multiple-quantum magnetization components. The theoretical background on the simultaneous detection of E.COSY-type, TROSY-type, or spin-edited multiplet patterns for different  $IS$  and  $I_2S$  spin systems in the same solution-state NMR spectrum is described. The proposed pulse scheme preserves high sensitivity levels and shows good tolerance to the presence of undesired cross-talk artifacts for both  $NH$  and  $NH_2$  multiplicities providing an interesting NMR tool for biomolecular applications.

### Introduction

Multidimensional NMR pulse sequences that exploit spin-state-selective ( $S^3$ ) properties in some way have emerged as powerful elements in modern NMR spectroscopy for the precise measurement of scalar and residual dipolar coupling constants<sup>1</sup> or also in the development of TROSY-type experiments<sup>2</sup> where only the most slowly relaxing of the four multiplet components of a typical  $IS$  cross-peak is observed. However, most of these actual  $S^3$  experiments exclusively work for  $IS$  spin systems and are based on the application of radio frequency pulses and fixed evolution delays, usually tuned to a specific  $J$  value, to achieve characteristic in-phase/antiphase (IP/AP) magnetization components that are conveniently combined during the pulse sequence. Often modified sequences must be used when applications on  $I_2S^3$  or  $I_3S^4$  spin systems are required.

Heteronuclear coherence transfer by means of heteronuclear cross-polarization (HCP)<sup>5</sup> provides additional and improved features over conventional pulse-interrupted free-precession

HMQC and HSQC pulse sequences. In this work, we report an INEPT-HCP pulse scheme (Figure 1) for the simultaneous observation of several types of  $S^3$  multiplet patterns for both  $IS$  and  $I_2S$  spin- $1/2$  systems from a single correlation spectrum. The typical E.COSY pattern or separate TROSY/anti-TROSY,  $F1-\alpha/\beta$  or  $F2-\alpha/\beta$  spin-state cross-peaks can be independently generated in a very straightforward manner using the same general pulse timing, with minor experimental changes and showing excellent tolerance to the presence of unwanted cross-talk artifacts for all types of  $S^3$  selection. The success of this approach relies on the fact that the anisotropic properties associated to HCP transfer afford high flexibility and versatility to manipulate specific IP/AP magnetization components in a very singular way<sup>5d</sup> and, in addition, combined with gradient echoes also enables the preservation of good sensitivity ratios for different  $I_nS$  multiplicities.<sup>6</sup>

### Experimental Section

All [<sup>15</sup>N,<sup>1</sup>H]-correlation NMR experiments were performed on a Bruker Avance 800 MHz spectrometer, equipped with a triple-resonance inverse TXI probe at 298 K. A sample of 1 mM <sup>13</sup>C,<sup>15</sup>N-doubly labeled ubiquitin dissolved in 90% H<sub>2</sub>O/10% D<sub>2</sub>O containing 50mM potassium phosphate buffer at pH 5.8 was used. For HCP transfer, two DIPSI-2 pulse trains were applied simultaneously to both <sup>1</sup>H and <sup>15</sup>N channels. An effective HCP bandwidth of  $\gamma B_1 = 2.8$  kHz (nominal 90° pulse of 90 $\mu$ s) offers excellent and uniform excitation over the complete NH regions of interest, 4 ppm for <sup>1</sup>H and 40 ppm for <sup>15</sup>N. However, in cases where a more effective HCP bandwidth should be required, a greater power lever would be applied at the expense of critical

<sup>†</sup> Universitat Autònoma de Barcelona.

<sup>‡</sup> Universitat de Barcelona.

- (1) Ding, K.; Gronenborn, A. M. *J. Magn. Reson.* **2003**, *163*, 208–214.
- (2) Pervushin, K.; Riek, R.; Wider, G.; Wüthrich, K. *Proc. Natl. Acad. Sci. U.S.A.* **1997**, *94*, 12366–12371.
- (3) (a) McIntosh, L. P.; Brun, E.; Kay, L. E. *J. Biomol. NMR* **1997**, *9*, 306–312. (b) Untidt, T. S.; Schulte-Herbrüggen, T.; Sorensen, O. W.; Nielsen, N. C. *J. Phys. Chem. A* **1999**, *103*, 8921–8926. (c) Permi, P. *J. Biomol. NMR* **2002**, *22*, 27–35. (d) Miclet, E.; O'Neil-Cabello, E.; Nikonowicz, E. P.; Live, D.; Bax, A. *J. Am. Chem. Soc.* **2003**, *125*, 15740–15741.
- (4) (a) Tugarinov, V.; Hwang, P. M.; Ollerenshaw, J. E.; Kay, L. E. *J. Am. Chem. Soc.* **2003**, *125*, 10420–10428. (b) Ollerenshaw, J. E.; Tugarinov, V.; Kay, L. E. *Magn. Reson. Chem.* **2003**, *41*, 843–862. (c) Kontaxis G.; Bax, A. *J. Biomol. NMR* **2001**, *20*, 77–82. (d) Pervushin, K.; Vögeli, B. *J. Am. Chem. Soc.* **2003**, *125*, 9566–9567.
- (5) (a) Bertrand, D. W.; Moniz, W. B.; Garroway, A. N.; Chingas, G. C. *J. Am. Chem. Soc.* **1978**, *100*, 5227–5229. (b) Ernst, M.; Griesinger, C.; Ernst, R. R.; Bermel, W. *Mol. Phys.* **1991**, *74*, 219–252. (c) Glaser, S.; Quant, J. *J. Adv. Magn. Opt. Reson.* (Ed. W. S. Warren) **1996**, *19*, 59–251. (d) Parella, T. *J. Biomol. NMR* **2004**, *29*, 37–55.

- (6) (a) Schleucher, J.; Schwendinger, M.; Sattler, M.; Schmidt, P.; Schedletsky, O.; Glaser, S. J.; Sorensen, O. W.; Griesinger, C. *J. Biomol. NMR* **1994**, *4*, 301–306. (b) Sattler, M.; Schmidt, P.; Schleucher, J.; Schedletsky, O.; Glaser, S. J.; Griesinger, C. *J. Magn. Reson. B* **1995**, *108*, 235–242. (c) Untidt, T.; Schulte-Herbrüggen, T.; Luy, B.; Glaser, S. J.; Griesinger, C.; Sorensen, O. W.; Nielsen, N. C. *Mol. Phys.* **1998**, *95*, 787–796.

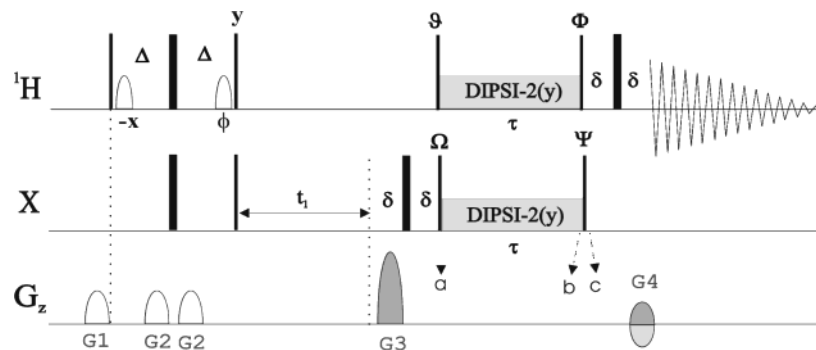


**Figure 1.** General pulse scheme for the sensitivity-enhanced  $^1\text{H}$ -X 2D spin-edited INEPT-HCP pulse sequence employed for recording the spectra presented in Figure 2. Narrow and wide pulses correspond to hard  $90^\circ$  and  $180^\circ$  flip angles, respectively, with phase  $x$  unless indicated. Water-selective pulses are indicated by shaped pulses in the  $^1\text{H}$  line. The phase  $\phi$  is individually set for each HCP version to ensure that water magnetization is along the  $+z$  axis during acquisition. The HCP mixing process (of duration  $\tau$ ) consists of a DIPSII-2 pulse train, applied from the  $y$  axis simultaneously to both  $^1\text{H}$  and X channels. Phases of  $90^\circ$  ( $^1\text{H}$ , X) pulses embedding the DIPSII-2 schemes: (A) Fully coupled:  $\vartheta = x$ ,  $\Omega = x$ ,  $\Phi = x$ , and  $\Psi$  = not applied. (B) E.COSY:  $\vartheta = x$ ,  $\Omega = x$ ,  $\Phi = x$ , and  $\Psi = x$ . (C and D) TROSY/anti-TROSY:  $\vartheta = -x/x$ ,  $\Omega = y$ ,  $\Phi$  = not applied, and  $\Psi = -x/x$ . (E and F) F2- $\alpha/\beta$  spin-edited acquired as described in phase C and D and applying a  $180^\circ$   $^1\text{H}$  pulse in the center of  $t_1$  to achieve heteronuclear decoupling in the F1 dimension. (G and H) F1- $\alpha/\beta$  spin-edited acquired as described in phase C and D but applying  $^{15}\text{N}$  GARP decoupling during acquisition.  $\Delta$  is set to  $1/4J(\text{IS})$ , and  $\delta$  is the gradient duration. See Table 1 for magnetization components available at time points a, b, and c in each version. G1 is a spoil gradient to remove any residual transverse magnetization prior to start the sequence, G2 belongs to the refocusing element, and coherence selection is achieved in a single scan using magic-angle G3 and G4 gradients. Echo-antecho data are acquired separately in an interleaved mode by inverting, in alternate scans, the gradient G4 and the phase  $\Omega$  in fully coupled and E.COSY versions, and  $\vartheta$  and  $\Psi$  in TROSY and  $\alpha/\beta$ -edited versions. The length and strengths of the sine-shaped gradients were as follows: G1( $x,y,z$ ) = 1 ms (0, 0, 11.74 G/cm); G2( $x,y,z$ ) = 1 ms (0, 0, 21.73 G/cm); G3( $x,y,z$ ) = 1 ms (26.08, 26.08, 26.08 G/cm); G4( $x,y,z$ ) = 1 ms (2.64, 2.64, 2.64 G/cm).

performance due to sample heating. The duration of the HCP mixing process ( $\tau$ ) was optimized at a compromised  $I_n\text{S}$  value of 9 ms which is equivalent to  $0.83/J$  for  $J = 92$  Hz. The radio frequency carrier offsets were placed at 8.0 ppm ( $^1\text{H}$ ), 118 ppm ( $^{15}\text{N}$ ), and 80 ppm ( $^{13}\text{C}$ ). The prescan and the interpulse  $\Delta$  delay were set to 1 s and  $1/4J(\text{NH})$  (2.7 ms), respectively, giving a total measuring time of 3 min for each 2D HCP spectrum. A  $500 \mu\text{s}$  adiabatic inversion pulse with a smoothed Chirp shape was applied in the center of  $t_1$  to remove the heteronuclear  $J(\text{NC})$  coupling splittings in the F1 dimension. The strong water signal was perfectly suppressed by using magic-angle gradients,<sup>7</sup> with a length of 1 ms and a recovery delay of  $100 \mu\text{s}$ . Water flip-back pulses of 1.5 ms with a Sinc shape were applied during the first INEPT block to avoid water saturation during acquisition, and the phases of these pulses must be optimized for each HCP version (see Supporting Information). The off-resonance effect of the HCP process on the water magnetization is considered null. The time domain data matrices consist of  $64 * 2\text{K}$  data points, with acquisition times of 9.9 ms ( $t_1$ ) and 106.6 ms ( $t_2$ ), and 2 transients per FID. Before Fourier transformation, the time domain data in the  $t_1$  and  $t_2$  dimensions were multiplied by a cosine function and zero-filled to  $512 * 2\text{K}$  data points, respectively.

### Theoretical Basis

For a given  $I_n\text{S}$  spin- $1/2$  system, the effective coupling term resulting from an HCP mixing sequence applied from the  $y$  axis can be approximately defined by the planar coupling tensor

$$H^{\text{eff}} = \frac{2\pi J_{\text{IS}}}{a} \left( \sum_{i=1}^n I_{iz} S_z + \sum_{i=1}^n I_{ix} S_x \right) \quad (1)$$

where the  $a$  constant is 2 and  $\sqrt{2}$  for IS and  $I_2\text{S}$  spin systems, respectively.<sup>5</sup> The most relevant transformations under the effect of the resulting planar TOCSY Hamiltonian<sup>5d</sup> (only sine-dependent terms are shown) can be summarized as

$$S_y \xrightarrow{HCP_y} \sum_{i=1}^n I_{iy} \sin^2 \left( \frac{\pi J_{\text{IS}} \tau}{a} \right) + \dots \quad (2a)$$

$$S_x \xrightarrow{HCP_y} \sum_{i=1}^n 2S_y I_{iz} \sin \left( \frac{\pi J_{\text{IS}} \tau}{a} \right) + \dots \quad (2b)$$

$$S_z \xrightarrow{HCP_y} - \sum_{i=1}^n 2S_y I_{ix} \sin \left( \frac{\pi J_{\text{IS}} \tau}{a} \right) + \dots \quad (2c)$$

And for two-spin IS product operators present before the HCP( $y$ ) mixing sequence:

$$\sum_{i=1}^n 2I_{iz} S_z \xrightarrow{HCP_y} \sum_{i=1}^n 2I_{iz} S_z \quad (2d)$$

$$\sum_{i=1}^n 2I_{iz} S_x \xrightarrow{HCP_y} \sum_{i=1}^n 2I_{ix} S_z \sin^2 \left( \frac{\pi J_{\text{IS}} \tau}{a} \right) + \dots \quad (2e)$$

$$\sum_{i=1}^n 2I_{iz} S_y \xrightarrow{HCP_y} - S_x \sin \left( \frac{\pi J_{\text{IS}} \tau}{a} \right) + \dots \quad (2f)$$

$$\sum_{i=1}^n 2I_{iy} S_z \xrightarrow{HCP_y} - \sum_{i=1}^n I_{ix} \sin \left( \frac{\pi J_{\text{IS}} \tau}{a} \right) + \dots \quad (2g)$$

$$\sum_{i=1}^n 2I_{iy} S_x \xrightarrow{HCP_y} \sum_{i=1}^n I_{iz} \sin \left( \frac{\pi J_{\text{IS}} \tau}{a} \right) + \dots \quad (2h)$$

$$\sum_{i=1}^n 2I_{iy} S_y \xrightarrow{HCP_y} \sum_{i=1}^n 2I_{iy} S_y \quad (2i)$$

$$\sum_{i=1}^n 2I_{ix} S_z \xrightarrow{HCP_y} \sum_{i=1}^n 2I_{iz} S_x \sin^2 \left( \frac{\pi J_{\text{IS}} \tau}{a} \right) + \dots \quad (2j)$$

(7) (a) Van Zij, P. C. M.; Johnson, M. O.; Mori, S.; Hurd, R. E. *J. Magn. Reson. A* **1995**, *113*, 265–270. (b) Warren W. S.; Richter, W.; Andreotti, A. H.; Farmer, B. T., II. *Science* **1993**, *262*, 2005–2009.

**Table 1.** Product Operators Present after Different Points of the Different INEPT-HCP Versions (Figure 1) Following the Variable  $t_1$  Evolution Time

Experiment	Time points			
	$t_1^a$	a	b <sup>c</sup>	c <sup>c</sup>
Fully-Coupled				$\sum_{i=1}^n 2I_{ix} * s$ $-\sum_{i=1}^n 2I_{iy} * s$ $+\sum_{i=1}^n 2I_{iy} S_y * s$ $-\sum_{i=1}^n 2I_{ix} S_y * s$
E.COSY	$\sum_{i=1}^n 2I_{iz} S_y \cos(\Omega_S t_1) \cos(\pi J_{IS} t_1)$ $-\sum_{i=1}^n 2I_{iz} S_x \sin(\Omega_S t_1) \cos(\pi J_{IS} t_1)$ $-S_x \cos(\Omega_S t_1) \sin(\pi J_{IS} t_1)$ $-S_y \sin(\Omega_S t_1) \sin(\pi J_{IS} t_1)$	$-\sum_{i=1}^n 2I_{iy} S_z$ $+\sum_{i=1}^n 2I_{iy} S_x$ $-S_x$ $-S_z$	$\sum_{i=1}^n 2I_{ix} * s$ $+\sum_{i=1}^n 2I_{iz} * s$ $-\sum_{i=1}^n 2I_{iz} S_y * s$ $-\sum_{i=1}^n 2I_{ix} S_y * s$	$\sum_{i=1}^n 2I_{ix} * s$ $-\sum_{i=1}^n 2I_{iy} * s$ $+\sum_{i=1}^n 2I_{iy} S_z * s$ $-\sum_{i=1}^n 2I_{ix} S_z * s$
TROSY (F1- $\alpha/\beta$ - edited) <sup>b</sup>		$-\sum_{i=1}^n 2I_{iy} S_y$ $+\sum_{i=1}^n 2I_{iy} S_z$ $+S_z$ $-S_y$	$-\sum_{i=1}^n 2I_{iy} S_y$ $-\sum_{i=1}^n 2I_{ix} * s$ $+\sum_{i=1}^n 2I_{iy} S_x * s$ $-\sum_{i=1}^n 2I_{iy} * s^2$	$-\sum_{i=1}^n 2I_{iy} S_z$ $-\sum_{i=1}^n 2I_{ix} * s$ $+\sum_{i=1}^n 2I_{iy} S_z * s$ $-\sum_{i=1}^n 2I_{iy} * s^2$
F2- $\alpha/\beta$ -edited	$\sum_{i=1}^n 2I_{iz} S_y \cos(\Omega_S t_1) -$ $\sum_{i=1}^n 2I_{iz} S_x \sin(\Omega_S t_1)$	$-\sum_{i=1}^n 2I_{iy} S_y$ $+\sum_{i=1}^n 2I_{iy} S_z$	$-\sum_{i=1}^n 2I_{iy} S_y$ $-\sum_{i=1}^n 2I_{ix} * s$	$-\sum_{i=1}^n 2I_{iy} S_z$ $-\sum_{i=1}^n 2I_{ix} * s$

<sup>a</sup> Trigonometric factors are shown only on this column. <sup>b</sup> Only the in-phase terms at point c are relevant. <sup>c</sup> The s factor stands for  $\sin(\pi J \tau / a)$ .

$$\sum_{i=1}^n 2I_{ix} S_x \xrightarrow{HCP_y} \sum_{i=1}^n 2I_{ix} S_x \quad (2k)$$

$$\sum_{i=1}^n 2I_{ix} S_y \xrightarrow{HCP_y} S_z \sin\left(\frac{\pi J_{IS} \tau}{a}\right) + \dots \quad (2l)$$

It can be deduced that maximum IP/AP heteronuclear transfer is generally achieved when the duration  $\tau$  of the mixing HCP process is adjusted to  $a/2J$ , which means  $1/J$ ,  $0.707/J$ , and  $0.6249/J$  for IS,  $I_2S$ , and  $I_3S$ , respectively.<sup>5</sup> This is in good agreement with the transfer efficiencies already known for the AP-to-IP heteronuclear coherence transfer achieved in HSQC and INEPT-HCP experiments.<sup>6</sup> As a basis for this work, we have used the INEPT-HCP pulse sequence (Figure 1) in order to study how the HCP mixing process manipulates the IP and AP coherences, belonging to different  $I_nS$  spin systems, present at the end of the variable  $t_1$  period. The effective Hamiltonian

generated by the overall mixing HCP process greatly depends on the role of all  $90^\circ$   $^1H$  and X pulses embedding the HCP sequence. A complete and detailed analysis of the different coherence transfer pathways for each particular HCP experiment has been already described.<sup>5d</sup> The proposed fully coupled INEPT-HCP experiment affords E.COSY or TROSY-type multiplet patterns by simple choice of the  $90^\circ$  hard I and S pulses (and their phases) embedding the HCP process. Alternatively, F1- $\alpha/\beta$  or F2- $\alpha/\beta$ -spin-edited experiments can also be recorded introducing heteronuclear decoupling during the variable  $t_1$  or acquisition periods, respectively, in the TROSY-HCP version. All these different transfer mechanisms are equally effective for other multiplicities than IS as summarized in Table 1. In addition, maximum sensitivity ratios are always achieved for all versions except for the F1-edited experiment where only two of the four possible mechanisms contribute to the observable magnetization.

**Table 2.** Theoretical Sensitivities for Selected and Suppressed Cross-Peaks in Spin-State Selective HCP Correlation Experiments

Experiment	Selected cross-peak	Suppressed cross-peak
E.COSY	$\frac{1}{2} \sin\left(\frac{\pi J_{IS}\tau}{a}\right)$	-
TROSY	$\frac{1}{4} \left[1 + \sin\left(\frac{\pi J_{IS}\tau}{a}\right)\right]^2$	Anti-TROSY: $\frac{1}{4} \left[1 - \sin\left(\frac{\pi J_{IS}\tau}{a}\right)\right]^2$ Semi-TROSY: $\pm \frac{1}{4} \left[1 - \sin^2\left(\frac{\pi J_{IS}\tau}{a}\right)\right]$
F1-spin-edited	$\frac{1}{2} \sin\left(\frac{\pi J_{IS}\tau}{a}\right) \left[1 + \sin\left(\frac{\pi J_{IS}\tau}{a}\right)\right]$	$\frac{1}{2} \sin\left(\frac{\pi J_{IS}\tau}{a}\right) \left[1 - \sin\left(\frac{\pi J_{IS}\tau}{a}\right)\right]$
F2-spin-edited	$\frac{1}{2} \left[1 + \sin\left(\frac{\pi J_{IS}\tau}{a}\right)\right]$	$\frac{1}{2} \left[1 - \sin\left(\frac{\pi J_{IS}\tau}{a}\right)\right]$

## Results and Discussion

The usefulness of the proposed approach was experimentally verified by obtaining several  $S^3$  editing patterns for both NH and  $NH_2$  spin systems in a series of  $^1H$ -coupled 2D  $^1H$ - $^{15}N$  INEPT-HCP correlation spectra acquired with a  $^{15}N$ ,  $^{13}C$ -labeled ubiquitin sample under the same experimental conditions (Figure 2).

In contrast to equivalent INEPT-based sequences, HCP achieves analogue coherence transfer pathways for all NH and  $NH_2$  moieties. The excellent spin-state selection for both NH and  $NH_2$  resonances is clearly visible from the E.COSY-HCP experiment using a compromise  $\tau$  value of 9 ms (Figure 2B). In addition to the well resolved  $^1J(NH)$ , this E.COSY pattern could allow the simultaneous measurement of geminal  $^2J(HH)$  coupling constants in  $I_2S$  moieties.<sup>8</sup> However, the 2-fold increase in the number of resonances that results when compared to conventional decoupled spectra can cause severe spectral crowding for large biomolecules. Simplified spectra can be recorded using equivalent alternatives that provide separate spin-edited subspectra as shown for TROSY/anti-TROSY (Figure 2C and D), F2- $\alpha/\beta$ -spin-edited (Figure 2E and F), and F1- $\alpha/\beta$ -spin-edited (Figure 2G and H) coupling patterns. For instance, the  $^1H$ - $^{15}N$  TROSY HCP experiment can be useful to detect simultaneously both backbone NH and side chain  $NH_2$  TROSY resonances from a single spectrum in large proteins.<sup>9</sup> Since the most efficient conditions for individual  $I_nS$  groups can be well established, an important aspect to regard is the cost paid in sensitivity and performance for the simultaneous detection of different multiplicities. Thus, experimental aspects such as the HCP length, the presence of cross-talk due to  $I_nS$ -averaged optimization, or the presence of different  $J_{IS}$  sizes should be taken into account. The sensitivity dependence of each selected/suppressed multiplet component in each spin-edited HCP transformation can be derived from the analysis of the transfer efficiencies (Table 2 and Figure 3).

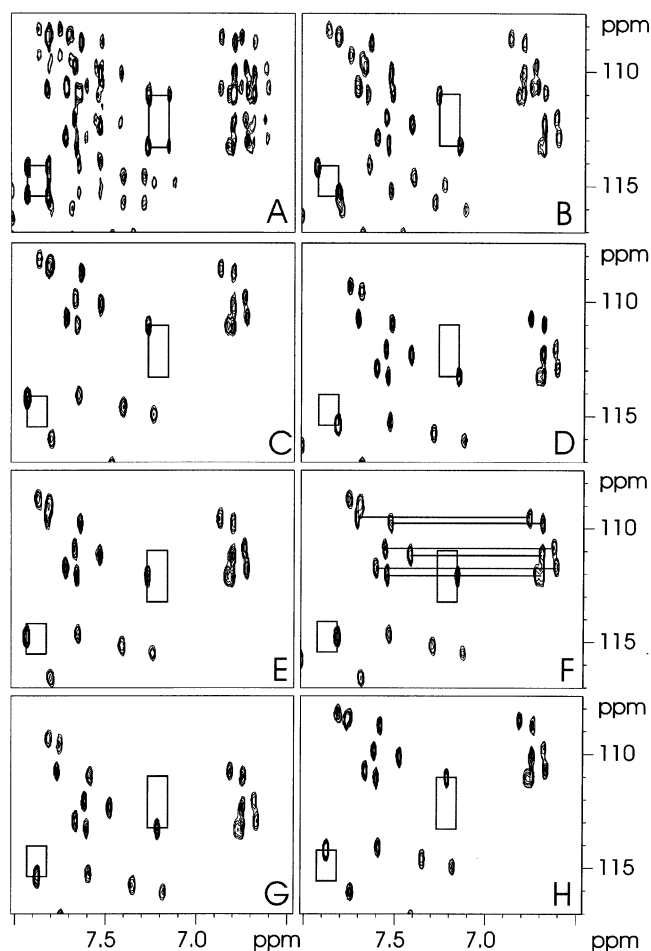


**Figure 2.** Expanded regions of several 2D  $^1H$ - $^{15}N$  INEPT-HCP spectra of 1 mM  $^{13}C$ ,  $^{15}N$ -doubly labeled ubiquitin in 90%  $H_2O$ /10%  $D_2O$  recorded at 800 MHz: (A) fully coupled, (B) E.COSY, (C) anti-TROSY, (D) TROSY, (E)  $\beta$ -F2-edited, and (F)  $\alpha$ -F2-edited, (E)  $\beta$ -F1-edited, and (F)  $\alpha$ -F1-edited. DIPSI-2 pulse trains (2.8 kHz) of 9 ms were used as HCP. A basic two-step phase cycling was used in which the first  $90^\circ(X)$  pulse was inverted with the receiver. 2 transients per FID were accumulated giving a total measuring time of 3 min for each 2D spectrum. Boxes are included for two target NH and  $NH_2$  resonances, and for clarity, seven  $NH_2$  resonances are distinguished in the F panel.

(8) Carlomagno, T.; Peti, W.; Griesinger, C. *J. Biomol. NMR* **2000**, *17*, 99–109.

(9) Pervushin, K.; Braun, D.; Fernández, S.; Wüthrich, K. *J. Biomol. NMR* **2000**, *17*, 195–202.

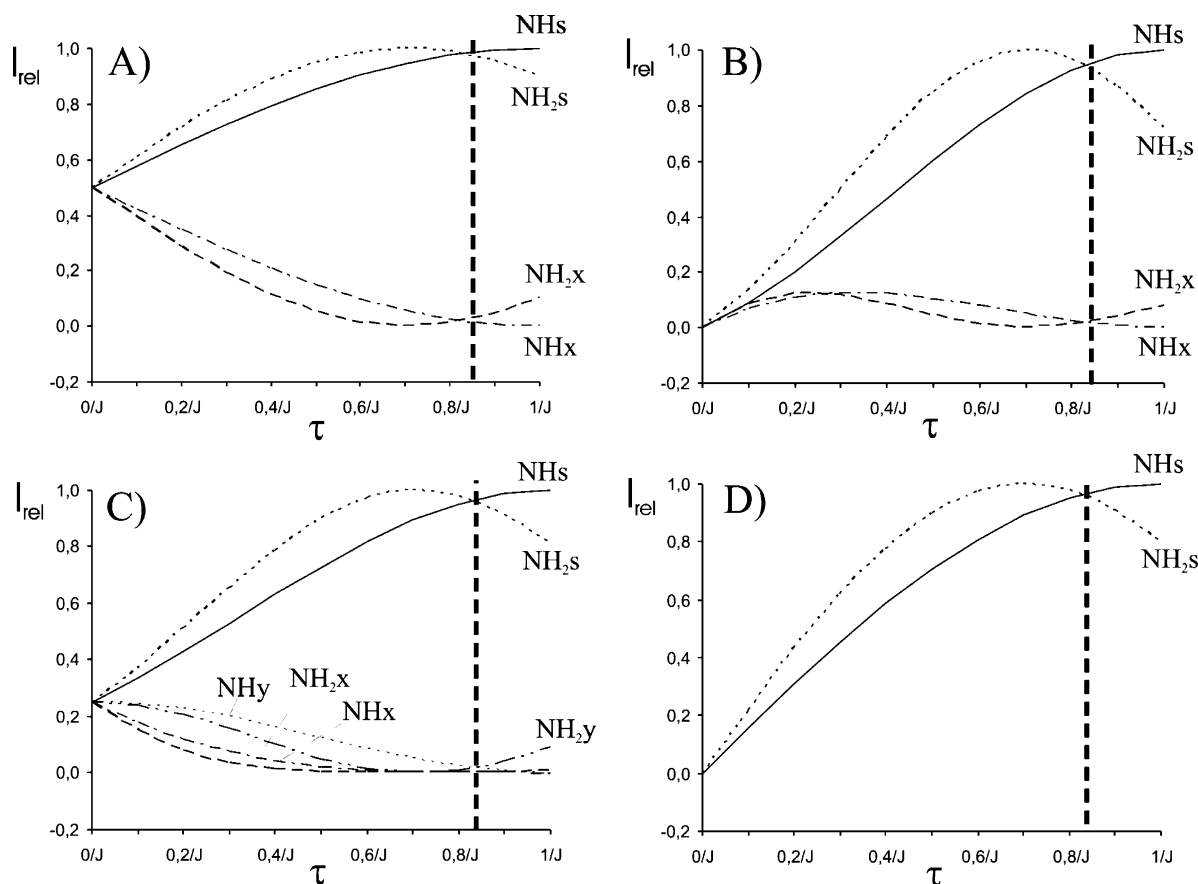


**Figure 3.** Curves illustrating the relative intensity dependence of the suppressed/selected signals in spin-state-selective INEPT-HCP experiments (Table 2) for IS and  $I_2S$  spin systems as a function of the HCP process duration ( $\tau$ ): (A) F2- $\alpha/\beta$ -spin-edited HCP; (B) F1- $\alpha/\beta$  spin-edited HCP; (C) TROSY-HCP; and (D) E.COSY-HCP. In all graphics, the selected cross-peaks for NH (—) and  $NH_2$  (---) are represented by the NHs and  $NH_2s$  lines, respectively. Suppressed cross-peaks for NH (---) and  $NH_2$  (---) are represented by the NHx and  $NH_2x$  lines, respectively. In the case of the TROSY version, the semi-TROSY cross-peaks for NH and  $NH_2$  are also shown as  $NH_y$  (---) and  $NH_{2y}$  (---), respectively.

The  $I_{\text{suppressed}}/I_{\text{selected}}$  ratio gives us an idea about the theoretical percentage of unwanted cross-talk artifacts present in each spectrum. Relaxation-induced contributions have not been considered in these equations. An important feature of the proposed HCP experiments is that the intensity of each NH multiplet component shows similar dependence as described for conventional INEPT-driven pulse schemes,<sup>11</sup> but as an additional feature, this behavior can also be expanded to  $NH_2$  resonances. The E.COSY-HCP experiment offers complete absence of cross-talk due to the compensation of all sine-dependent terms in the suppressed IS and  $I_2S$  cross-peak, and therefore the experiment only suffers from possible sensitivity losses due to unmatched  $\tau$  optimization (Figure 3D).

As shown in all graphics of Figure 3, a theoretical HCP duration about  $0.835/J$  gives excellent results in terms of  $I_nS$ -optimized sensitivity and minimum presence of cross-talk artifacts for NH and  $NH_2$  resonances. Under these conditions the theoretical loss of sensitivity and the presence of unwanted cross-talk contribution do not exceed a 5% level for both NH and  $NH_2$  resonances in the more sensitive F1-spin-edited HCP experiment (Figure 3B). Cross-talk percentages are lower than 2.5–3% in the other versions. As an example, Figure 4 shows

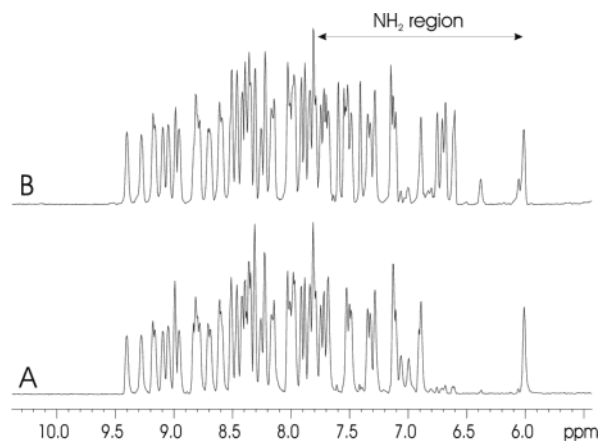


**Figure 4.** F2 projections of (A) a conventional gradient echo-antiecho TROSY experiment and (B) TROSY-HCP experiment as recorded in Figure 2D. Note the absence of cross-talk for both NH and  $NH_2$  resonances.

the comparison of F2 projections of the HCP-TROSY experiment of Figure 2D with an equivalent TROSY experiment using an echo-antiecho gradient for coherence selection.<sup>10</sup> It can be quickly observed that NH cross-peaks are obtained with similar intensity, and as an extra bonus, the  $NH_2$  resonances also appear with good sensitivity and minimum cross-talk contributions. Figure 5 shows some 1D sections taken at different  $^{15}NH$  and  $^{15}NH_2$  frequencies of the most robust F2-spin-edited HCP experiment, in which only very small cross-talk contributions

(10) (a) Czisch, M.; Boelens, R. *J. Magn. Reson.* **1998**, *134*, 158–160. (b) Weigelt, J. *J. Am. Chem. Soc.* **1998**, *120*, 10778–10779.  
 (11) (a) Cordier, F.; Dingley, A. J.; Grzesiek, S. *J. Biomol. NMR* **1999**, *13*, 175–180. (b) Meissner, A.; Schulte-Herbrüggen, T.; Briand, J.; Sorensen, O. W. *Mol. Phys.* **1998**, *95*, 1137–1142.

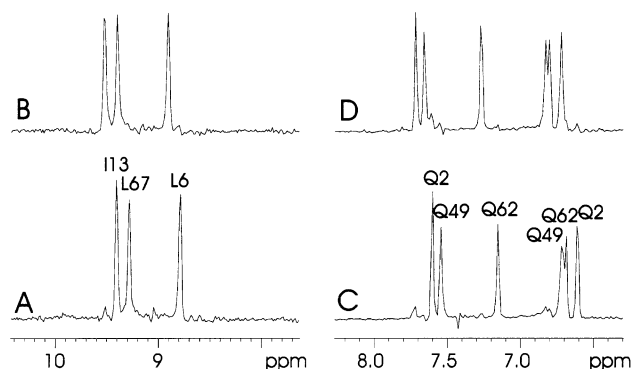


**Figure 5.** Experimental 1D F1 slices taken at the  $^{15}\text{N}$  chemical shift frequency of different NH (A,B) and  $\text{NH}_2$  (C,D) frequencies from the (A,C)  $\alpha$ -F2-edited and (B,D)  $\beta$ -F2-edited INEPT-HCP spectra already described in Figure 2E and F.

are observed as theoretically predicted (Figure 3A). In this case, the ratio

$$\frac{I_{\text{suppressed}}}{I_{\text{selected}}} = \frac{1 - \sin(\pi J\tau/a)}{1 + \sin(\pi J\tau/a)} \approx \frac{(\pi\Delta J\tau/a)^2}{4}$$

gives an approximate value of the cross-talk percentage as a function of the coupling deviation,  $\Delta J$ , and  $\tau$  settings.<sup>11a</sup>

The INEPT-HCP pulse sequence presented here offers maximum sensitivity ratios because of the combination of gradient-echoes with the PEP approach.<sup>12</sup> Since gradients provide coherence selection, a single scan per  $t_1$  value is sufficient to record clean 2D spectra and therefore a gradient echo–antiecho HCP element can be easily implemented in multidimensional NMR pulse schemes. The INEPT-HCP scheme can also take profit of other interesting features already exploited in INEPT-based experiments. For instance, the water flip-back approach must be incorporated during the initial INEPT block to minimize water saturation.<sup>13</sup> The phases of these  $90^\circ$  selective water pulses must be individually set for each spin-state HCP version in order to put the water magnetization to its equilibrium position ( $+z$  axis) at the beginning of the acquisition period. To enhance the overall sensitivity of HCP experiments, the  $^{15}\text{N}$  steady-state magnetization can be also merged to the conventional  $^1\text{H}$  steady-state magnetization if the initial INEPT block is not phase-cycled. In the case of ubiquitin, the expected 10% sensitivity increase is achieved (see supplementary info) but better results should be obtained in cases where  $T_1(^{15}\text{N})$  is shorter than  $T_1(^1\text{H})$ .<sup>13–14</sup> Another important aspect which is away of the scope of this work is the relaxation induced effects occurring during the HCP mixing process. A detailed analysis of the relaxation effects of SQ  $^1\text{H}$  and  $^{15}\text{N}$  coherences and MQ coherences under spin-lock conditions will be required, and careful evaluation of different relaxation rates or cross-correlation effects between the different mechanisms can have high

impact on the application of HCP experiments on large biomolecules.<sup>15</sup> Different approaches could also be applicable into HCP experiments for the attenuation of cross-talk contribution due to relaxation effects as described for INEPT-type sequences, such as the complementary-E.COSY approach in which cross-correlation of passive spins is compensated<sup>16</sup> or the clean-TROSY experiment in which a modified mixing sequence is used to quench peaks of opposite phase.<sup>17</sup>

## Conclusions

In summary, we have shown that E.COSY-type, TROSY-type, and  $\alpha/\beta$  spin-edited coupling patterns for different IS and  $\text{I}_2\text{S}$  spin systems can be simultaneously obtained in the same HCP correlation spectrum. It is also worth mentioning that all principles outlined here demonstrate that HCP promises to be a valuable and efficient mixing NMR element as an alternative to common INEPT-based blocks and they could also be expanded to analogue phase-cycled HCP experiments that do not use pulsed-field gradients for coherence selection. As occurred for the basic HSQC pulse sequence, further developments on the proposed HCP pulse schemes will permit improvement of their sensitivity, performance, and design of new possible applications. Important aspects such as the differential relaxation properties and cross-correlation effects between the involved magnetizations and the behavior in the presence of chemical exchange phenomena under spin-locking conditions must be evaluated in more detail. The potential ability to suppress conformational exchange contributions to the resonance line width, the application to the measurement of different scalar and residual dipolar coupling constants, and, in particular, the possibility to retrieve a variety of structural information simultaneously from backbone NH (CH) and side chain  $\text{NH}_2$  ( $\text{CH}_2$ ) spin systems will be also of high interest. The successful application of the principles described here on  $\text{CH}_3$  methyl groups must be evaluated in more detail and will be properly addressed in the future work.

**Acknowledgment.** Financial support for this research provided by MCYT (Project BQU2003-01677) is gratefully acknowledged. We thank the Servei de Resonància Magnètica Nuclear, UAB, and Unitat de RMN dels Serveis de Suport a la Recerca, UB, for allocating instrument time to this project.

**Supporting Information Available:** Pulse sequences of all proposed INEPT-HCP experiments. Spectra showing the experimental  $^1\text{H}$  and  $^{15}\text{N}$  steady-state contributions to the overall sensitivity. This material is available free of charge via the Internet at <http://pubs.acs.org>.

JA0495866

- (12) Kay, L. E.; Keifer, P.; Saarinen, T. *J. Am. Chem. Soc.* **1992**, *114*, 10663–10665.  
 (13) Pervushin, K. V.; Wider, G.; Wüthrich, K. *J. Biomol. NMR* **1998**, *12*, 345–348.

- (14) (a) Riek, R. *J. Biomol. NMR* **2001**, *21*, 99–105. (b) Pervushin, K.; Riek, R.; Wider, G.; Wüthrich, K. *J. Am. Chem. Soc.* **1998**, *120*, 6394–6400. (c) Brutscher, B.; Boisbouvier, J.; Pardi, A.; Marion, D.; Simorre, J. P. *J. Am. Chem. Soc.* **1998**, *120*, 11845–11851.  
 (15) Rance, M.; Loria, J. P.; Palmer, A. G., III. *J. Magn. Reson.* **1999**, *136*, 92–101.  
 (16) Meissner, A.; Schulte-Herbrüggen, T.; Sorensen, O. W. *J. Am. Chem. Soc.* **1998**, *120*, 7989–7990.  
 (17) Schulte-Herbrüggen, T.; Sorensen, O. W. *J. Magn. Reson.* **2000**, *144*, 123–128.